

# 3D-Printed Paper Spray Ionization Cartridge with Integrated Desolvation Feature and Ion Optics

G. IJ. Salentijn,<sup>†,‡,§</sup> R. D. Oleschuk,<sup>§</sup> and E. Verpoorte<sup>\*,†</sup>

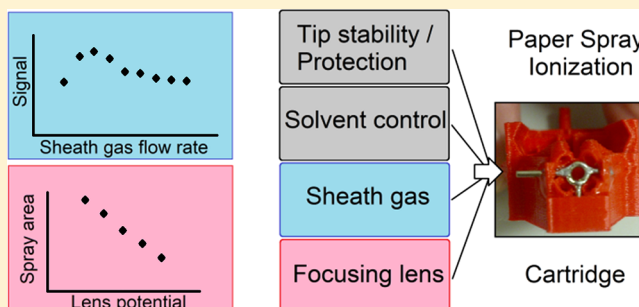
<sup>†</sup>Pharmaceutical Analysis, Groningen Research Institute of Pharmacy, University of Groningen, Groningen, The Netherlands

<sup>‡</sup>TI-COAST, Science Park 904, 1098 XH Amsterdam, The Netherlands

<sup>§</sup>Department of Chemistry, Queen's University, Kingston, Ontario, Canada

## Supporting Information

**ABSTRACT:** In this work we present the application of 3D-printing for the miniaturization and functionalization of an ion source for (portable) mass spectrometry (MS). Two versions of a 3D-printed cartridge for paper spray ionization (PSI) are demonstrated, assessed, and compared. We first focus on the use of 3D-printing to enable the integration of an embedded electrostatic lens and a manifold for internal sheath gas distribution and delivery. Cartridges with and without a sheath gas manifold and an electrostatic lens are compared with respect to analytical performance and operational flexibility. The sensitivity and limit of detection are improved in the cartridge with an electrostatic lens and sheath gas manifold compared to the cartridge without (15% and over 6.5× smaller, respectively). The use of these focusing elements also improved the average spray stability. Furthermore, the range of potentials required for PSI was lower, and the distance to the MS orifice over which spray could be obtained was larger. Importantly, both setups allowed quantification of a model drug in the ng/mL range with single-stage MS, after correction for spray instability. Finally, we believe that this work is an example of the impact that 3D-printing will have on the future of analytical device fabrication, miniaturization, and functionalization.



In the world of engineering technology, 3D-printing is a “rising star”. This collection of fabrication techniques has made a huge impact on the consumer market, where we are seeing a shift from buying e.g. gadgets, trinkets, and functional objects to printing them yourself. The concept of *rapid prototyping* has also been completely reinvented with this development, making a strong impact in many scientific fields, with the potential to revolutionize the way we do research. In the field of microfluidics, we also see these trends;<sup>1–6</sup> 3D-printing is now being used for many purposes, importantly to fabricate analytical devices, and to customize lab equipment or setups. Still, there is a lot of room left to increase the level of ingenuity and complexity of 3D-printed devices for chemical analysis. Device geometries are often still relatively simple and could, in many cases, be achieved via other fabrication methods (at least, if the costs associated with device prototyping and fabrication could be neglected).

In 2014, we published a functionalized 3D-printed cartridge for an ambient ionization technique called paper spray ionization (PSI).<sup>7</sup> PSI is becoming more popular due to its simplicity and low cost. Many reports have described the use of PSI for the quantification of, for example, drugs of abuse,<sup>8</sup> pharmaceuticals in blood,<sup>9,10</sup> and toxicants and pollutants in foodstuffs.<sup>11</sup> It is striking that many, if not all, of these methods have two things in common: (i) no use of desolvation gases, but rather a heated capillary inlet for the liberation of gas-phase

ions, and (ii) the use of tandem MS for quantification (we found one exception, but the analyses were in the mM-range<sup>12</sup>). This may be explained by the fact that the use of PSI is still mostly in the development phase, and therefore standardized sources are not yet widespread, even though they are commercially available.<sup>8</sup> Customized PSI interfaces to the MS are still the rule, and paper tips are often positioned with a metal clip, without the possibility of using sheath gas or the integration of additional functionality in the source. The use of desolvation gases is beneficial in instruments without heated-capillary inlets, but from an engineering point-of-view more difficult to achieve reproducibly. Furthermore, due to the nature of the paper substrate (i.e., a porous network of cellulose fibers) and the production method of the tips (i.e., manual cutting), reproducible paper tips, and thus reproducible and stable spray, are often difficult to obtain. Finally, spray is typically only obtained for a minute or so, due to solvent depletion.<sup>13</sup> For these reasons, people are relying on the fragmentation of analytes (tandem MS) and internal standards to perform quantitative analysis.<sup>14</sup>

With the establishment of the PSI approach, further functionalization of the paper tips has attracted increased

Received: June 27, 2017

Accepted: October 4, 2017

Published: October 17, 2017

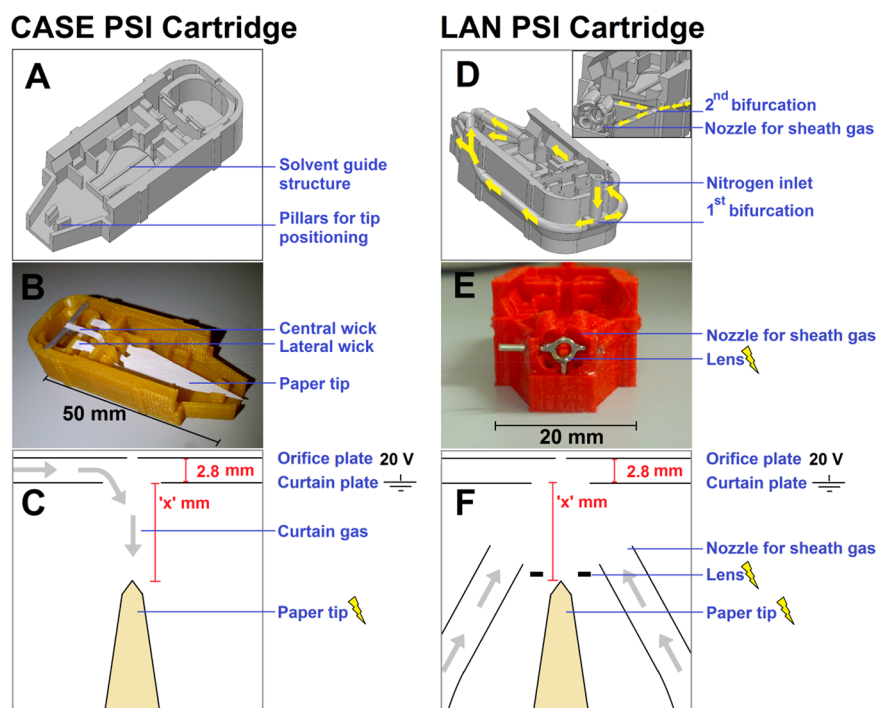


**Figure 1.** (A–C) PSI cartridge configuration for controlled and symmetric elution (CASE). (D–F) PSI cartridge with electrostatic lens and nozzles for sheath gas delivery (LAN). The figure shows (A, D) the Solidworks design, (B, E) a 3D-printed device (without the lid), and (C, F) schematic top views of the experimental configurations for PSI. Yellow arrows in D show the distribution of air through the network of ducts, bifurcations and nozzles; the inset in D shows a cross-sectional front view along the length of the gas tubes.

attention. Early examples focused on the on-paper chemical derivatization of compounds to increase ionization efficiency<sup>13</sup> or the use of alternative substrates to improve analytical performance<sup>15,16</sup> (generally by employing substrates with different porosities or surface energy). More recently, “high” throughput PSI has been demonstrated<sup>17</sup> as well as the integration of simple paper microfluidic structures on paper tips to improve the method performance.<sup>12,18,19</sup> However, many of these examples are not user-friendly, and the success of the functionalization is limited by the nature of the PSI method itself.

Cartridge-based PSI can be employed to improve user-friendliness and allow easier integration of functionality. Recent achievements include the implementation of better solvent control<sup>7</sup> and solid phase extraction.<sup>20</sup> In this work, we expand the capabilities and level of integration of a PSI cartridge, in such a way that is not feasible with traditional (micro)-fabrication techniques. Two novel versions of a 3D-printed cartridge for PSI were designed, fabricated, and tested. The first represents an upgraded version of a cartridge design we reported in 2014 and integrates features for fast wetting and continuous solvent supply to the paper tip.<sup>7</sup> The second version incorporates several additional features to enhance performance, including an electrostatic lens, and pneumatic ducts and nozzles for sheath gas delivery. In both versions, desolvation gases (either as curtain gas or as sheath gas) are employed to improve signal, and quantitative analysis in single-MS mode is demonstrated. While improving and/or expanding the possibilities and applicability of PSI is definitely an objective of this work, the main impact and innovation lie in the design and realization of the two upgraded 3D-printed cartridge designs. The cartridges exhibit a high level of integration, which would not have been possible without additive manufacturing.

## MATERIALS AND METHODS

**Chemicals and Disposables.** Polylactic acid (PLA, Easyfil, Formfutura, Nijmegen, The Netherlands) was the material of choice in the fused-deposition-modeling (FDM) 3D-printing process. Grade-1 chromatography paper (Whatman, Maidstone, England) was used to make the paper tips. Methanol (Biosolve B.V., Valkenswaard, The Netherlands) with 1% formic acid (v/v) (Sigma-Aldrich, Steinheim, Germany) and a few drops of blue food dye (mix of E133 and E122) was used as the spray solvent for the characterization of the spray focusing effect of the electrostatic lens. Prilocaine (MW. 220, 20  $\mu\text{M}$  in water) was used as a model compound for optimization experiments. Different concentrations of lidocaine (MW. 234; 0.05–10  $\mu\text{M}$  in water) were used in quantification experiments, with prilocaine (20  $\mu\text{M}$ ) as an internal standard (see Supporting Information (SI), Figure S1 for structural formulas). In every PSI-MS experiment, a sample volume of 5  $\mu\text{L}$  was spotted onto the front of the tip and dried before analysis. 480  $\mu\text{L}$  of methanol with 1% formic acid (v/v) was used as eluent and spray solvent in PSI-MS experiments.

**Cartridge Designs.** Two different cartridges were produced and tested for a number of characteristics. The first cartridge was an improved version of the fast wetting and continuous solvent supply (FWACSS) PSI cartridge that was published in 2014.<sup>7</sup> The improvements were as follows (see Figure 1A–B, and SI, Figure S2). Two lateral wicks (one on each side of the central wick) instead of just one wick served to provide continuous wetting. The three wicks lead to a symmetrical flow profile and increased supply of solvent during the experiment (which is particularly important for solvents with a high contribution of volatile, organic solvent such as methanol). Second, a platform, on which the base of the paper tip could rest, served as a solvent guide structure, as well as a

secondary reservoir for excess solvent from the fast initial wetting. Toward the front of the cartridge, the tip was suspended in air, allowing slower migration of solvent through the paper and thus a controlled elution of sample to the front of the tip. Third, the contact between the front of the tip and the cartridge was minimized, to prevent unwanted solvent and sample retention in undesirable locations around the tip. This cartridge model is henceforth referred to as a controlled and symmetric elution (CASE) PSI cartridge. Furthermore, a 3D-printed holder for the cartridge was developed, which could be directly mounted onto the front of the mass spectrometer, to increase the reproducibility of cartridge positioning (see SI, Figure S2). This cartridge was tested with curtain gas (i.e., gas flow in the direction opposite to the direction of the spray) from the mass spectrometer (Figure 1C).

The second cartridge was tested with two more implemented features (Figure 1D–E). Four nozzles were included around the spray tip for the continuous delivery of sheath gas, supplied to the cartridge sheath gas manifold via a single inlet at the rear of the cartridge. Additionally, an electrostatic lens was included as a focusing element immediately in front of the paper tip. This cartridge model is henceforth referred to as the *lens and nozzles* (LAN) PSI cartridge. The same 3D-printed holder affixed to the MS was used for positioning as was employed for the CASE PSI cartridge. However, sheath gas was used instead of curtain gas for the operation of the LAN cartridge (Figure 1F).

**Fabrication.** The 3D drawing and fabrication of PSI cartridges is described in detail in previous work.<sup>7</sup> In short, designs were made in Solidworks (Waltham, MA, USA) and exported in \*STL format. This file was sliced (Skeinforge/SFact), and then the part was printed on a Felix v. 3 FDM 3D printer (Felix, de Meern, The Netherlands), run by Repertier Host firmware.

The electrostatic lens was made by bending a nickel-plated paperclip ( $d = 0.8$  mm) around a metal rod ( $d = 1.5$  mm) and subsequently cutting the thus-formed spiral into circles. Each circle was closed with solder, and three wire arms were attached to the circle for positioning it in the front end of the 3D-printed cartridge and for connection to a power supply (see Figure 1E). The lens was inserted by pausing the 3D printer at a specific point during the print job, in which a predesigned cavity for the lens had been formed. After placement of the lens, the print was resumed and the cavity for the lens was sealed from above, thus confining the lens to the cartridge.

The inlet for sheath gas was designed with an inner diameter of 1.5 mm and an outer diameter of 3 mm. The inner diameter of the manifold (with curves and bifurcations) varied roughly between 1.4 and 1.6 mm. In order to test for leakages in the air ducts, air was guided through the cartridge while submerging it in a water bath. If present, leaks were identified and sealed by applying two-component epoxy glue to the exterior of the ducts.

Paper tips were cut using a 3D-printed stencil and a surgical scalpel. The front part of the tips were cut at an angle of  $60^\circ$  (see Figure 1C and 1F) using a pressing rather than a slicing motion of the blade, to prevent cellulose fibers from being pulled apart. The tips were inspected under the microscope, and frayed ends were removed with a scalpel. Furthermore, the two corners at the front of the tip were rounded off to prevent spray and discharge between those corners and the electrostatic lens.

**Characterization of Air Distribution over Four Nozzles (LAN PSI Cartridge).** The path lengths and diameters along the four different conduits were designed to be identical for sheath gas flow in the desolvation network. In order to quantify the actual distribution of air after fabrication through the bifurcations and ducts of the 3D-printed network, an adapted version of the LAN PSI cartridge was designed and printed with extended nozzles, so that flexible tubes could be attached (see Figure 2A). Four lengths of tubing were cut to the same length

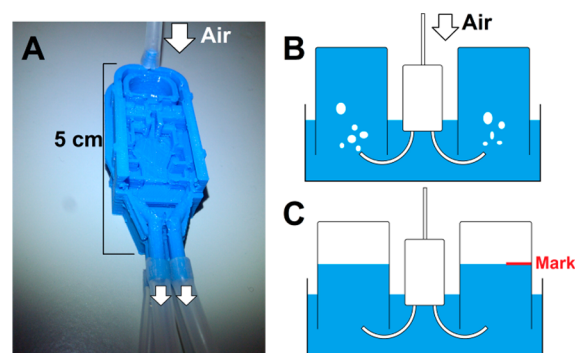


**Figure 2.** Setup for the characterization of the air distribution from a single inlet through three bifurcations and finally four exit nozzles. (A) The LAN PSI cartridge was adapted and equipped with extended nozzles for the attachment of tubing. (B) Each piece of tubing was placed beneath the opening to a water-filled bottle, which was positioned up-side-down in a water bath. Upon application of air (0.2 bar), the water was forced out of the bottles and replaced by air. (C) After approximately 30 s, the level of the water–air interface was marked on the bottle and read to approximate the volume of displaced water.

and these were attached to the cartridge. Four bottles with volumetric markings were filled completely with water and submerged into a water bath, top-down (see Figure 2B). Each of the four tubes extending from a nozzle was placed under the opening of a bottle. Next, the air inlet of the cartridge was connected to an air source (0.2 bar) and air flow was applied (see SI, Video S1). After approximately 30 s, the gas flow was stopped and a mark was made on each bottle at the level of the water–air interface inside the bottle (Figure 2C). The volume in each bottle occupied by air was related to the average volume of air in the four bottles in that run, yielding a relative distribution. This was repeated two more times with the same cartridge ( $n = 3$ ), and an average percentage per nozzle was calculated. The standard deviation of the four nozzles was calculated to determine the distribution of air from a single inlet over the four nozzles.

**Characterization of the Electrostatic Lens (LAN PSI Cartridge).** The effect of the electrostatic lens was visualized by introducing spray solvent with blue dye added to a LAN PSI cartridge, which was then positioned in front of a metal plate at ground potential. Different potentials (200–700 V,  $n = 3$  per potential) were applied to the lens while the paper tip was kept at the same potential (2.3 kV) and spray was generated for approximately 2 min per condition. After 2 min, the lens potential was altered and the cartridge was shifted a few millimeters along the plate. The spots were then photographed with a ruler for size reference. ImageJ<sup>21</sup> was used to measure the height and width of the spots, which were used to approximate the area.

**PSI Setup.** PSI-MS experiments were performed on a Sciex API 2000. When coupled to a standard electrospray ion source, desolvation is ensured by the use of elevated temperature and both sheath and curtain gas. In our experiments, elevated temperatures were not used, as that would damage the 3D-printed plastics. For the CASE PSI cartridge, curtain gas was applied via the MS. A flow regulator was built between the nitrogen source and the MS inlet. A flow rate of 0.3 L/min was used, as higher flow rates generally impaired paper spray, whereas lower flow rates led to lower signal (probably because of less desolvation). For the LAN PSI cartridge, the nitrogen tubing was detached from the MS and attached to the cartridge's sheath gas network. The opening for curtain gas in the MS inlet was sealed with a cap. Sheath gas flow rates between 0.7 and 1.5 L/min were applied. In both setups, the curtain plate was grounded. PSI cartridges were positioned reproducibly with a specifically designed 3D-printed holder that could be clicked onto the MS (see SI, Figure S2).

**Data Processing and Analysis.** Data from all PSI-MS experiments were recorded with Analyst software in the  $m/z$  range of 50–500 (1 s acquisition time for the entire range). The total ion current (TIC) and extracted ion chromatogram (XIC) traces for  $m/z$  221 and 235 (signals for protonated prilocaine and lidocaine, respectively) were exported as text files. These files were imported into Microsoft Excel, which was used for simple data processing. The ratios for 221/TIC and 235/221 were calculated and plotted over time. Since the concentration of prilocaine (221) was kept constant in all experiments, the 221/TIC ratio was used as a measure for spectral complexity. This allows the quantification of the ratio between informative and noninformative MS data. The 235/221 ratio was used for quantification of lidocaine samples. In the 221/TIC plot, a threshold value was selected as a minimum filter to exclude noninformative data (0.025–0.06 in CASE cartridges (average of 0.041); 0.04–0.15 in LAN cartridges (average of 0.091) in quantification experiments (see SI, Tables S1, S2). The first 50 of the remaining data points were subsequently used to (i) determine 221/TIC, (ii) quantify lidocaine ( $m/z$  235/221), and (iii) assess spray quality. The latter was done by calculating (a) the time it took to acquire those 50 data points (shorter acquisition times mean more informative data, thus better signal stability) and (ii) the relative standard deviation (RSD) of the 50 data points on the prilocaine trace (XIC of  $m/z$  221), which was used for this purpose because it was the internal standard in our experiments. The (a) acquisition times and (b) RSD values of the absolute signal on the 221 trace for each experiment were combined into a data set (either CASE or LAN). Both data sets have their own mean and SD. A two-tailed  $t$  test was used to assess whether the data sets were significantly different.

**Setup Optimization.** For both configurations (CASE and LAN), the distance between the tip and the curtain plate was varied ( $x = 1.8, 2.8, 3.8, \text{ or } 4.8$  mm; see Figure 1C and 1F) and aqueous samples containing only prilocaine (20  $\mu\text{M}$ ) were analyzed to determine the 221/TIC ( $n = 3$  or higher). Curtain gas and sheath gas flow rates were set at 0.3 and 0.9 L/min, respectively, for these analyses.

In the next set of experiments, the flow rate of the sheath gas in the LAN PSI cartridge was varied during the elution of prilocaine. Since the compound is spotted on paper and eluted during the experiment, the concentration (and thus the 221/TIC) changes over time. When a stable spray had been obtained at a nitrogen sheath flow rate of 0.9 L/min, the

experiment was started. After approximately 15 s, the sheath gas flow rate was changed to a different value. Approximately 15 s later, it was changed back to 0.9 L/min. This procedure was repeated for each of the tested sheath flow rates. The 221/TIC values for tested sheath flow rates were normalized with respect to values of 221/TIC obtained at 0.9 L/min, recorded just before and after each test point.

The lens potential was fixed at 500 V, which is in between the potential of the paper (>1.5 kV) and the curtain plate (ground).

**Quantitative Analysis with Single-Stage MS.** Calibration lines were measured for the analysis of lidocaine with both the CASE PSI cartridge ( $x = 1.8$  mm, curtain gas flow rate = 0.3 L/min) and the LAN PSI cartridge ( $x = 3.8$  mm, sheath gas flow rate = 0.9 L/min, lens potential = 500 V), after the above-mentioned data processing step. Sensitivity was calculated as the slope of the calibration lines. The limit of detection (LOD) and quantification (LOQ) were obtained by multiplying the SD of five blank samples (containing only prilocaine) with 3 and 10, respectively, and dividing them by the sensitivity.

## RESULTS AND DISCUSSION

**Characterization of Air Distribution over Four Nozzles (LAN PSI Cartridge).** Airflow was obtained from all four nozzles when air was applied to the single inlet of the sheath gas manifold (see SI, Video S1). The experiment was performed in triplicate, and an RSD of 11% was obtained for flows through the different nozzles (see SI, Figure S3). In the experiment, we reproducibly found the same flow ratios when comparing the different nozzles (i.e., one nozzle consistently emitted the highest gas flow, and another consistently emitted the lowest). The deviation from a completely equal distribution over all four nozzles can be attributed to different flow resistances of the respective gas ducts, which in turn are caused by minor differences in the actual diameter of the ducts. We can account for this difference by recalling that we are pushing the limit of the 3D printer resolution at this small scale, which is in the order of a few hundred micrometers. The use of a 3D-printing approach with a higher resolution should lead to a more equal distribution. Nevertheless, the distribution is still acceptable, and the (spatial) control over gas flows is likely greater than would be the case in a configuration in which desolvation gases would have had to be applied via fixed, external tubes in a cartridge-less setup. Furthermore, the network for gas delivery does not consist of simple straight tubes, but of curved, bifurcating, ascending and descending ducts (see Figure 1D, yellow arrows).

**Characterization of the Electrostatic Lens (LAN PSI Cartridge).** A spray visualization experiment was performed, in which spray solvent with a blue dye was sprayed against a metal plate through the electrostatic lens. Different lens potentials were tested with respect to a fixed potential applied to the paper tip. This led to the formation of differently sized blue spots on the grounded plate (see Figure 3A). The width and height of these spots were measured and plotted as a function of the applied potentials (see SI, Figure S4). Next, the spot area was calculated and also plotted as a function of the applied potentials (see Figure 3B). In all cases, we see a clear correlation between the dimensions and the applied potential. The lens can therefore be used to focus the ion spray, since the spray spots become smaller with an increase in lens potential. However, increasing the lens potential with respect to a fixed potential applied to the paper tip effectively decreases the

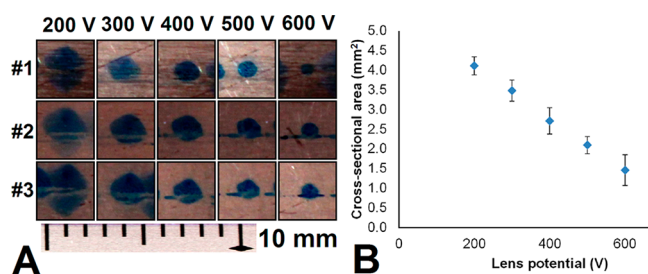


**Figure 3.** Characterization of the electrostatic lens in a LAN PSI cartridge. (A) Spray solvent with blue dye was sprayed onto a metal plate. Potentials of 200–600 V (in triplicate) were applied to the lens, while the potential between the tip and the metal plate was kept fixed (2.3 kV). (B) Relationship between applied lens potential and cross-sectional area of paper spray, which decreases at a higher lens potential. Error bars show the standard deviation.

electric field strength available for PSI. Since a sufficiently strong electric field is required to generate paper spray, a maximum lens potential was encountered above which spray could no longer be generated (600–700 V).

**Data Processing.** In order to do quantitative analysis with single-stage PSI-MS, it is necessary to perform some data treatment prior to analysis. Data from most spray experiments contain both periods during which good spray signal was obtained (informative data), as well as periods during which no signal or signal from poor spray was recorded (noninformative data). This is due to the fact that PSI is often not stable, which can lead to strong fluctuations in signal amplitudes, as well as very noisy spectra. In turn, this means that we need to find a way to distinguish between informative and noninformative spectra. Figure S5 (SI) shows an example of a spray experiment in which we clearly see both types of data. It also shows how the inclusion of such data might lead to incorrect results, and how applying a filter based on the 221/TIC prior to data analysis resolved the issue.

Another approach for quantification using an internal standard would involve taking the ratio between the areas under the curve for the traces of lidocaine (sample) and prilocaine (internal standard). Even in an unfiltered set of data, the contribution from noninformative data would only be minor, because the individual signals are added before the ratio is taken and these signals are negligible compared to signal from informative spectra. However, with the approach delineated in Figure S5 in the SI, there is better control over the quality of the data that are used. By filtering the data based on the 221/TIC, noninformative data points are discarded and data analysis begins when actual analyte signals have been observed.

#### Positioning of the Cartridge in Both Configurations.

Table 1 shows the obtained 221/TIC values for both cartridge configurations (CASE and LAN) at different distances from the curtain plate, as well as the range of potentials that had to be applied in order to obtain paper spray. If we compare both cartridges at the same distance from the MS ( $x = 2.8$  mm), Table 1 shows that use of the LAN PSI cartridge results in a cleaner (3.1 times higher 221/TIC,  $p < 0.05$ , two-tailed  $t$  test, paired variance) signal than the CASE model and requires a lower spray potential (up to 2 kV). In this comparison, the cleaner signal resulted mainly from a significant decrease in total ion signal, whereas the absolute analyte signal remained of similar magnitude. The difference in required potentials between the two configurations is probably based on the

**Table 1.** Influence of the Position of the Cartridge in Both Configurations

Configuration	Distance ( $x$ ) to the curtain plate (mm)	$n$	221/TIC <sup>a</sup> $\pm$ SD	Potential range (kV)
CASE PSI cartridge, curtain gas (0.3 L/min)	2.8	3	$0.054 \pm 0.018$	3–4
	1.8	5	$0.058 \pm 0.014$	2–3
LAN PSI cartridge, sheath gas (0.9 L/min)	4.8	3	$0.11 \pm 0.032$	1.5–2.2
	3.8	5	$0.13 \pm 0.016$	1.5–2.2
	2.8	3	$0.17 \pm 0.014$	1.5–2.2

<sup>a</sup>Used as the ratio between informative and noninformative data.

distribution of the electrical field. In the CASE PSI cartridge, the electrical field at the tip decreases with an increased distance between the tip and curtain plate (increased “ $x$ ” in Figure 1C). Therefore, increasingly high potentials are required to produce spray, up to the point where spray can no longer be obtained (starting above 2.8 mm) with potentials up to 5 kV. In the LAN model, the distance between the lens and the paper tip is constant, regardless of the position of the cartridge; thus, the electrical field at the tip is less influenced by the distance between the tip and curtain plate (“ $x$ ” in Figure 1F). This results in a situation where spray could still be obtained at a distance of 4.8 mm from the curtain plate and a potential range which appears to be unaffected by the value of “ $x$ ”. Greater distances were not tested, due to the fact that the 221/TIC ratio decreased as the distance to the curtain plate increased.

An increase of the 221/TIC with a shorter distance to the orifice is observed for both configurations, probably due to the fact that the diameter of the cross-section of the spray increases as it travels to the MS inlet. Therefore, analyte becomes more spread out, as a longer distance to the MS is chosen. A drawback of positioning either cartridge close to the MS orifice is the decreased control of positioning in the other two dimensions. The reason for this is simple, namely that the cartridge is so close to the curtain plate that we can no longer see where the paper tip and the center of the lens are “pointing”.

#### Influence of Sheath Gas Flow Rate on 221/TIC in the LAN Configuration.

Figure 4 demonstrates how the sheath gas flow rate influences the PSI signal. The prilocaine and total ion trace are plotted over time for an experiment in which sheath gas flow rates were alternated between 0.9 L/min and other values (Figure 4A). Black arrows indicate when the flow rate was changed to a different value for 15 s, after which it was changed back to 0.9 L/min for 15 s (indicated by a smaller, light-blue arrow). The average 221/TIC for all of those 15-s windows are plotted over time (Figure 4B). The blue line in 4B, which connects all the windows taken at 0.9 L/min, shows the elution profile of prilocaine from the paper tip. Furthermore, it shows that the 221/TIC values for all other flow rates (red diamonds) lie below this line. In Figure 4C, the values for all the different sheath gas flow rates in Figure 4B are normalized with respect to the blue line (i.e., the interpolated elution profile of prilocaine at 0.9 L/min). This was done by taking the ratio between the value of interest (red diamonds) and the average of the two neighboring values on the 0.9 L/min curve (blue diamonds). Figure 4C visualizes the relation between sheath gas flow rate and 221/TIC for the entire flow rate range.

Sheath gas may affect ion intensity in two respects. First of all, desolvation is facilitated by convective air movement. Higher flow rates would lead to more evaporation and thus

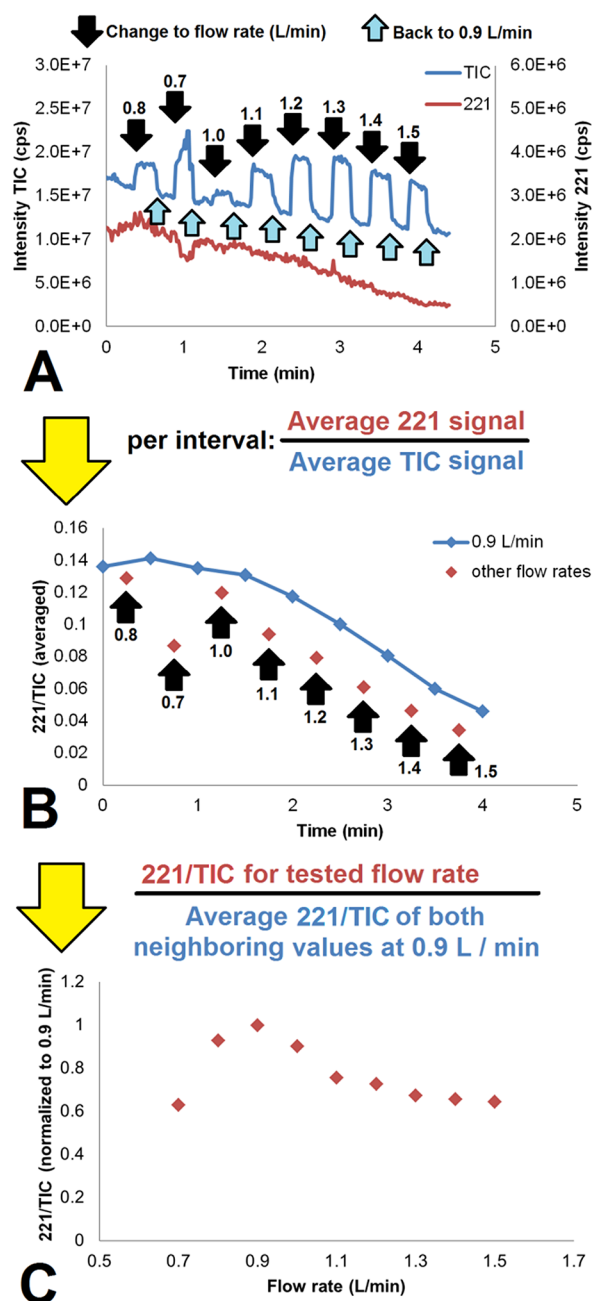


**Figure 4.** Influence of sheath gas flow rate on 221/TIC for the LAN PSI cartridge ( $20 \mu\text{M}$  prilocaine in water,  $5 \mu\text{L}$ ). (A) TIC and 221 trace. (B) 221/TIC ratio over time and (C) normalized 221/TIC (with respect to the 221/TIC found at 0.9 L/min directly before and after the flow rate measurement in question) versus the sheath gas flow rate. During the experiment, the flow rate was switched from and back to 0.9 L/min. Labeled black arrows indicate at which times the flow rate was changed and into which value. Light-blue arrows indicate when the sheath gas flow rate was changed back to 0.9 L/min.

faster and more efficient formation of gas-phase ions. Moreover, as the nozzles are designed with an inward angle, the nitrogen will aid in focusing the spray. At lower flow rates, this effect could be beneficial, yet at higher flow rates, adverse effects due to turbulence may occur, which could impair stable spray. Furthermore, excessive focusing could also lead to an increase in unwanted signal (such as that stemming from solvent molecules).

There is an optimum in the sheath gas flow rate range at 0.9 L/min. At lower flow rates, we see a higher total signal, while the analyte signal decreases. This probably means that the desolvation is less efficient (less prilocaine is liberated, higher solvent signals are observed). At higher flow rates, the 221/TIC also drops, but this is caused mainly by an increase in total signal, whereas the contribution of changes in the prilocaine signal are low. Most likely, there is sufficient desolvation, but additional focusing of the ion cloud occurs, leading to a higher total signal. If we are not applying sheath gas, or at a very low flow rate, it becomes difficult to obtain spray in this configuration.

Finally, it is important to note that the experiments in this work were all performed with methanol as spray solvent, which evaporates relatively easily, compared to water. Therefore, the choice of a sheath gas flow rate should be optimized for different compositions of the spray solvent.

**Quantification of Lidocaine with Single-Stage MS (CASE and LAN PSI Cartridges).** Figure 5 shows the calibration lines for lidocaine in water for both setups, with concentrations up to  $5 \mu\text{M}$ . The performance of both methods is also summarized in Table 2. An overview of the individual experiments, with values listed for important parameters (including 221/TIC, 235/221, and thresholds for data filtration), can be found in Tables S1 and S2 in the SI, for the CASE model and the LAN model, respectively. These combined results demonstrate that the LAN PSI cartridge gives a higher sensitivity (15% increase) than the CASE model, and the LOD and LOQ for the LAN model are also improved (>6.5 times lower). Along with the lower required potentials for spray generation, and increased flexibility of cartridge positioning, these numbers show that the LAN PSI cartridge has enhanced performance compared to the CASE model. On a more general note, these results show that quantitative analysis is feasible with both cartridges, even without resorting to tandem MS, at least for this particular analysis. More research is needed to allow more general statements about the quantitative performance and applicability in different contexts, but that is beyond the scope of this work.

**Signal Quality.** Table 2 also shows that the LAN PSI cartridge appears to give a better spray stability than the CASE model, likely due to the directional focusing of ions by both the electrostatic lens and the sheath gas. Experiments with the LAN PSI cartridge showed significantly smaller signal fluctuations (based on the mean of RSDs of the absolute signal in the prilocaine trace after filtration,  $n = 20$ ) compared to the CASE model (>3 times lower,  $p \ll 0.05$  (two-tailed  $t$  test, unpaired variance)), but there was no significant difference found in the time it took to generate 50 spectra of sufficient quality ( $p = 0.176$  (two-tailed  $t$  test, paired variance)). There is still some variation in the quality of the experiments with the LAN PSI cartridge, which occasionally resulted in poor spray and thus in differences in the quality of the experiments. This may be attributed to the fact that the lens was handmade, and the paper tips are still manually cut and positioned in the cartridge. If the tip is not completely symmetrical, misaligned in the cartridge, or some cellulose fibers are sticking out, stable spray may be impaired. Furthermore, the experiments with the CASE PSI cartridge generally required continuous tuning of the potential to obtain proper signal, often over a range of approximately 1 kV, whereas the LAN configuration commonly required only a single, fixed potential.

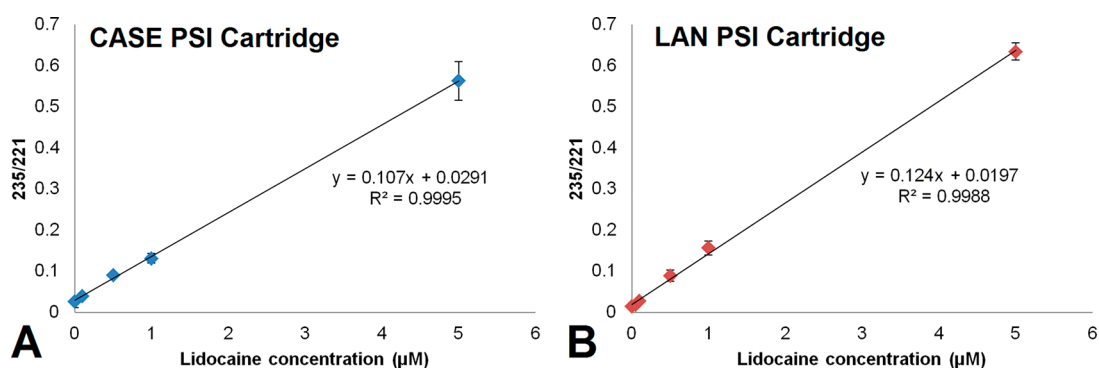


**Figure 5.** Quantification of lidocaine with internal standard (prilocaine, 20  $\mu\text{M}$ ) in water with single-stage MS, using the (A) CASE and (B) LAN PSI cartridges.

**Table 2.** Quantification of Lidocaine in Water with the CASE and LAN Cartridges and 20  $\mu\text{M}$  Prilocaine as Internal Standard

Configuration	Lidocaine concentration range (nM)	Sensitivity	LOD (nM)	LOQ (nM)	LOD (ng/mL)	LOQ (ng/mL)	Time between 1st and 50th data point (min)	Average RSD on the 221 trace (%) $\pm$ SD
CASE PSI Cartridge, curtain gas (0.3 L/min)	100–5000	0.107	415	$1.38 \times 10^3$	97.1	324	$1.44 \pm 0.67$ ( $n = 20$ )	$31.5 \pm 14.0$ ( $n = 20$ )
LAN PSI Cartridge, sheath gas (0.9 L/min)	50–5000	0.124	62	206	14.5	48.3	$1.18 \pm 0.49$ ( $n = 20$ )	$9.4 \pm 5.5$ ( $n = 20$ )

## CONCLUSION

The concept of 3D-printing gas ducts and nozzles opens new design possibilities for customized experimental setups, as it can be employed for techniques other than PSI. Normally, the generic ion source of an MS is removed when an experimental setup is created to develop a new ion source technology, which limits the possibilities of even using sheath gas. With 3D-printing, a preferred duct and nozzle angle can be realized more quickly, releasing the gas at the optimal location. Furthermore, we have shown that 3D-printing allows the integration of non-3D-printed objects into a single part (e.g., an electrostatic lens). This is also an attractive feature of employing 3D-printing for the fabrication of miniaturized instrumentation.

Cartridge-based PSI was employed for quantitative analysis using only single-stage mass spectrometry, which could be used to detect and quantify an aqueous solution of lidocaine in the ng/mL range, after facile data processing. Obviously, whether single MS suffices is highly application-specific and, for the analysis of very complex samples, the use of tandem MS would in all likelihood still be necessary. Further and more detailed assessment of the quantitative performance of the PSI cartridges should therefore be performed in a case-by-case fashion. We have also developed a cartridge for PSI into which a sheath gas function and an electric lens have been integrated (LAN configuration). The performance (3 $\times$  cleaner signal, 15% sensitivity increase, >6.5 $\times$  lower LOD) and signal stability (>3 times lower RSD on  $m/z$  221 traces) were improved when compared with the cartridge without these functions (CASE configuration). Furthermore, spray could be generated at lower potentials and over larger distances with these additions, giving the user more flexibility. These developments may also benefit the field of miniaturized mass spectrometry, in which a fully portable MS is the goal.

In order to further increase the reproducibility of paper spray measurements, the process of cartridge and lens fabrication, as well as cutting and positioning of the paper tip, should be automated. Currently, the main cause for inferior measurements seems to be the imprecision associated with the manual

fabrication process (differential cutting, misalignment of the tip, imperfections in the lens).

Significant PSI cartridge optimization was carried out, but a number of parameters could still be explored to produce a further enhanced PSI signal. First of all, only a single configuration for the nozzles was tested. Different angles to the axis of the spray and different positions in relation to the front of the paper tip might lead to better focusing and desolvation of analyte ions. Second, additional ion optics might be integrated in order to better guide ions toward the orifice of the MS. Finally, the size and shape of the paper tip is an important parameter for the quality of the spray, as has been demonstrated in other studies,<sup>22</sup> and we believe that there is still room for improvement in this field. However, we have shown that mastering the incorporation of signal enhancing features such as sheath gas and an electric lens into the PSI cartridge can compensate in part for imperfections in the paper tip.

## ASSOCIATED CONTENT

### Supporting Information

The Supporting Information is available free of charge on the ACS Publications website at DOI: 10.1021/acs.analchem.7b02490.

Air inlet of the cartridge connected to an air source (0.2 bar) with air flow applied (AVI)

Structural formulas of lidocaine and prilocaine, additional information about the cartridge design, and characterization experiments, and an overview of the data of the quantification experiments (PDF)

## AUTHOR INFORMATION

### Corresponding Author

\*E-mail: e.m.j.verpoorte@rug.nl.

### ORCID

G. IJ. Salentijn: 0000-0002-2870-9084

R. D. Oleschuk: 0000-0003-2783-7532

### Author Contributions

The manuscript was written through contributions of all authors. All authors have given approval to the final version of the manuscript.

### Notes

The authors declare no competing financial interest.

### ACKNOWLEDGMENTS

This research received funding from The Netherlands Organization for Scientific Research (NWO) in the framework of the Technology Area COAST (Project Number 053.21.108). We would like to thank the Mass Spectrometry Core Facility, University of Groningen, and in particular Dr. H.P. Permentier, for their assistance.

### REFERENCES

- (1) Yazdi, A. A.; Popma, A.; Wong, W.; Nguyen, T.; Pan, Y.; Xu, J. *Microfluid. Nanofluid.* **2016**, *20*, 1–18.
- (2) Au, A. K.; Huynh, W.; Horowitz, L. F.; Folch, A. *Angew. Chem., Int. Ed.* **2016**, *55*, 3862–3881.
- (3) Ho, C. M. B.; Ng, S. H.; Li, K. H. H.; Yoon, Y.-J. *Lab Chip* **2015**, *15*, 3627–3637.
- (4) O'Neill, P. F.; Ben Azouz, A.; Vázquez, M.; Liu, J.; Marczak, S.; Slouka, Z.; Chang, H. C.; Diamond, D.; Brabazon, D. *Biomicrofluidics* **2014**, *8*, 052112.
- (5) Gross, B. C.; Erkal, J. L.; Lockwood, S. Y.; Chen, C.; Spence, D. *M. Anal. Chem.* **2014**, *86*, 3240–3253.
- (6) Salentijn, G. IJ.; Oomen, P. E.; Grajewski, M.; Verpoorte, E. *Anal. Chem.* **2017**, *89*, 7053–7061.
- (7) Salentijn, G. IJ.; Permentier, H. P.; Verpoorte, E. *Anal. Chem.* **2014**, *86*, 11657–11665.
- (8) Espy, R. D.; Teunissen, S. F.; Manicke, N. E.; Ren, Y.; Ouyang, Z.; Van Asten, A.; Cooks, R. G. *Anal. Chem.* **2014**, *86*, 7712–7718.
- (9) Manicke, N. E.; Abu-Rabie, P.; Spooner, N.; Ouyang, Z.; Cooks, R. G. *J. Am. Soc. Mass Spectrom.* **2011**, *22*, 1501–1507.
- (10) Manicke, N. E.; Yang, Q.; Wang, H.; Oradu, S.; Ouyang, Z.; Cooks, R. G. *Int. J. Mass Spectrom.* **2011**, *300*, 123–129.
- (11) Zhang, Z.; Cooks, R. G.; Ouyang, Z. *Analyst* **2012**, *137*, 2556–2558.
- (12) Colletes, T. C.; Garcia, P. T.; Campanha, R. B.; Abdelnur, P. V.; Romão, W.; Coltro, W. K. T.; Vaz, B. G. *Analyst* **2016**, *141*, 1707–1713.
- (13) Liu, J.; Wang, H.; Manicke, N. E.; Lin, J.-M.; Cooks, R. G.; Ouyang, Z. *Anal. Chem.* **2010**, *82*, 2463–2471.
- (14) Ferreira, C. R.; Yannell, K. E.; Jarmusch, A. K.; Pirro, V.; Ouyang, Z.; Cooks, R. G. *Clin. Chem.* **2016**, *62*, 99–110.
- (15) Zhang, Z.; Xu, W.; Manicke, N. E.; Cooks, R. G.; Ouyang, Z. *Anal. Chem.* **2012**, *84*, 931–938.
- (16) Narayanan, R.; Sarkar, D.; Cooks, R. G.; Pradeep, T. *Angew. Chem., Int. Ed.* **2014**, *53*, 5936–5940.
- (17) Shen, L.; Zhang, J.; Yang, Q.; Manicke, N. E.; Ouyang, Z. *Clin. Chim. Acta* **2013**, *420*, 28–33.
- (18) Damon, D. D.; Maher, Y. S.; Yin, M.; Jjunju, F.; Young, I. S.; Taylor, S.; Maher, S.; Badu-Tawiah, A. K. *Analyst* **2016**, *141*, 3866–3873.
- (19) Salentijn, G. IJ.; Hamidon, N. N.; Verpoorte, E. *Conference on Miniaturized Systems for Chemistry and Life Sciences (MicroTAS)*; 2016; pp 1308–1309.
- (20) Zhang, C.; Manicke, N. E. *Anal. Chem.* **2015**, *87*, 6212–6219.
- (21) Schneider, C. A.; Rasband, W. S.; Eliceiri, K. W. *Nat. Methods* **2012**, *9*, 671–675.
- (22) Yang, Q.; Wang, H.; Maas, J. D.; Chappell, W. J.; Manicke, N. E.; Cooks, R. G.; Ouyang, Z. *Int. J. Mass Spectrom.* **2012**, *312*, 201–207.